

Design of Qubit Readout Circuit for Purcell Rate Suppressing and Nonclassicality Enhancing

Ahmad Salmanoglu^{1*}, Hesam Zandi^{2,3,4}, Saeed Hajihosseini³, Mahdi Esmaeili³, M. Hossein Eskandari³, and Mohsen Akbari⁵

¹Ankara Yildirim Beyazit University, Engineering Faculty, Electrical and Electronic Department, Ankara, Turkey

²Faculty of Electrical Engineering, K.N. Toosi University of Technology, Tehran, Iran

³Iranian Quantum Technologies Research Center (IQTEC), Tehran, Iran

⁴Electronic Materials Laboratory, K.N. Toosi University of Technology, Tehran, Iran

⁵Quantum Optics Lab, Department of Physics, Kharazmi University, Tehran, Iran

AhmadSalmanoghli@aybu.edu.tr

Abstract

The Purcell effect, a common issue in qubit-resonator systems leading to both fidelity and nonclassicality losses is studied while its suppression is achieved using a novel qubit readout circuit design. Our approach utilizes a unique coupling architecture in which, the qubit first interacts with a filter resonator before coupling to the readout resonator. This configuration enables precise control over the Purcell decay rate and ac Stark factor without impacting on measuring time. The mentioned factor is highly sensitive to the coupling strength between the readout resonator and the filter, meaning that the factor adjustment directly impacts the qubit state detection. A major advantage of this design is that tuning the resonator-filter coupling strength is relatively straightforward, offering flexibility in fine-tuning ac Stark factor. This work extensively analyzes the system using full quantum mechanical theory, deriving the total Hamiltonian and investigates mode dynamics via quantum Langevin equations. Key parameters influencing the nonclassicality of output signals are also explored through quantum correlation metrics, including symplectic eigenvalues, quantum discord, and classical discord. The main goal is to find any compromises existing between the ac Stark factor (2χ) increasing and the quantum correlation created in the readout circuit. By optimizing the critical factors, by which the ac Stark factor mainly affected, the proposed design not only improves the distinguishability of the qubit states but also ensures robust nonclassicality in the output signals. Results demonstrate the potential of the proposed system to bridge the gap between a high fidelity readout and quantum correlation preservation in scalable quantum architectures.

Key words: Purcell rate, Purcell filter, Quantum circuit, Entanglement metric, Nonclassicality, Quantum discord

1. Introduction

Homodyne detection has emerged as a prominent technique for measuring the state of a qubit, relying on the detection of state-dependent frequency shifts in a resonator coupled to the qubit [1]. However, this method faces significant challenges, primarily due to the Purcell effect [2], which describes the energy leakage resulting from the resonator's coupling to the qubit and its subsequent decay [1, 3-4]. This phenomenon critically influences the overall performance of the measurement process, as it can substantially degrade the readout fidelity [5]. The Purcell rate, a metric quantifying the energy dissipation from the qubit via the resonator, presents a fundamental challenge to achieve high-fidelity qubit state

measurements. To mitigate energy leakage, the first strategy involves increasing the detuning between the resonator and the qubit, effectively reducing the energy transfer rate, while alternatively, decreasing the coupling strength between the qubit and the resonator can also alleviate the Purcell effect [6, 7]. However, both strategies entail inherent trade-off between the qubit relaxation and measurement time. Raising the resonator detuning extends the duration required for qubit state measurements, potentially compromising the system's overall efficiency [8-10]. Conversely, diminishing the qubit-resonator coupling can diminish the probability of achieving entanglement, a crucial aspect in quantum computing and communication systems [11-13].

Addressing these challenges is essential for optimizing measurement fidelity while preserving the entanglement properties necessary for robust quantum information processing. To address these inherent trade-offs, the introduction of a Purcell filter has proven beneficial [14,15]. This device is engineered to selectively control energy leakage from the qubit through the resonator, without significantly compromising the coupling strength or detuning. By integrating a filter resonator between the qubit and the readout resonator, the system can effectively suppress unwanted energy loss while preserving strong qubit-resonator interactions [16-18]. This enables high-fidelity measurements, ensuring that entanglement probabilities remain intact and measurement times are optimized. The implications of these strategies are particularly critical in the context of scalable quantum architectures, where enhancing measurement fidelity is paramount for achieving reliable quantum operations across multiple qubits. Along with, to attain the main goal of this work, this study extensively explores the quantum correlation and nonclassicality of signals [19-27] with a focus on designing a quantum circuit that enhances the distinguishability of the qubit's state via the readout circuit. The ultimate goal is to accurately determine the state of a single qubit or coupled qubits, a task achieved through an appropriate readout circuit. Moreover, the nonclassical nature of output signals is equally significant. This work not only investigates the key parameters influencing the performance of the readout circuit in detecting the qubit state with high fidelity but also examines factors affecting the nonclassicality of the output signals. To achieve this, several quantum correlation criteria, including the symplectic eigenvalue [21, 25-27], quantum discord [28-30], and classical discord, are analyzed in the context of the proposed quantum system. In the following, we will study our new design and delve deeper into the concepts and difference with the traditional one.

2. Theory and Method

In this design, schematically illustrated in Fig. 1, unlike the traditional Purcell filter circuit [3, 7], the qubit is first coupled to the filter resonator, and then the coupled system is weakly connected to the readout resonator. Therefore, the qubit modes are coupled to the filter modes and eventually the output modes are coupled to the main resonator. This means that the resonator sense the Purcell filter output, instead of the qubit mode. The new design

also brings some new degrees of freedom to manipulate the Purcell rate completely effectively. Indeed, this work paves way to develop of higher fidelity qubit readout procedures. To show the abilities of the new design, it will be comprehensively analyzed and especially its mode dynamics will be investigated using full quantum theory.

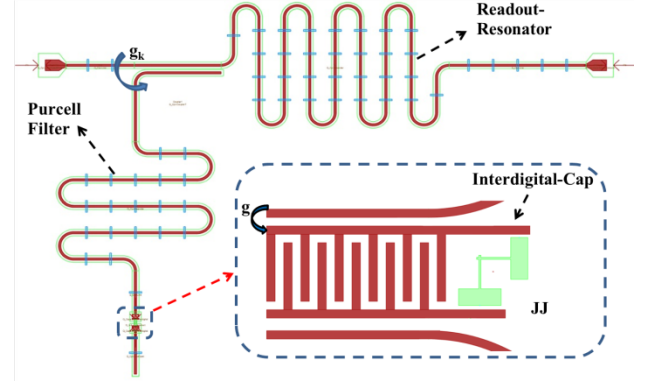


Fig 1. The layout of the circuit containing the readout resonator, Purcell filter, interdigital capacitor, and Josephson Junction (JJ), zoomed in the inset plot.

The main concern is how much the new design can enhance the readout resonator fidelity along with how much the non-classicality is being affected. For complete analysis of the system, we utilized a full quantum mechanical approach [19-22]. Theoretically deriving the total Hamiltonian can be presented as:

$$\begin{cases} H_0 = \omega_r a^\dagger a + \omega_f b^\dagger b + \omega_q \sigma_z / 2 \\ H_{\text{int}} = g_k (a^\dagger + a)(b^\dagger + b) + g (a^\dagger + a)(\sigma^+ + \sigma^-) \end{cases} \quad (1)$$

where $(\omega_r, \omega_f, \omega_q)$, $g_k, g, \kappa_r, \kappa_{\text{eff}}, \gamma_s$, (a^\dagger, a) , (b^\dagger, b) , σ^+ and σ^- are, readout resonator, Purcell filter, qubit angular frequency, coupling between Purcell filter and readout resonator, qubit and Purcell filter coupling factor, readout resonator decay rate (measurement coupling factor), modified decay rate of qubit due to the coupling to Purcell filter, qubit spontaneous emission, and readout resonator, Purcell filter, and qubit raising and lowering operators, respectively. Using the derived Hamiltonian, the system's dynamics equation of the motion (quantum Langevin equation) [19] is become:

$$\begin{cases} \dot{a} = -i\omega_r a - ig_k b - \kappa_f a / 2 + \sqrt{2\kappa_f} \varepsilon_{in} \\ \dot{b} = -i\omega_f b - ig_k a - ig \sigma^- \\ \dot{\sigma}^- = i\omega_q \sigma^- - ig \sigma_z b \\ \dot{\sigma}_z = -\gamma_z (\sigma_z + I) - 2ig (b^+ \sigma^- - b \sigma^+) \end{cases} \quad (2)$$

where ε_{in} is the drive of the resonator. Consequently, one can calculate the modified decay rate of the qubit coupling to the Purcell filter (qubit Purcell rate) [7], κ_{eff} , by merging the equations of (2) as:

$$\kappa_{eff} = \frac{4|g_k|^2}{\kappa_f} \cdot \frac{1}{1 + (2\Delta_r/\kappa_f)^2} + \frac{\gamma_s}{N_f} \cdot \frac{1}{1 + (\gamma_s \Delta_q / |g|^2 (N_f + 1))^2} \quad (3)$$

where N_f is the average number of photons in the Purcell filter resonator, $\langle b^+ b \rangle$. In this equation, the first term is the same factor that has been derived and studied earlier in the literature [3-7]; it shows that through engineering the coupling between the resonator and the Purcell filter along with the measurement decay, it becomes possible to manipulate the qubit decay. Detuning between the resonator and driving is also another factor that can strongly affect κ_{eff} . It should be noted that in the Eq. 8 of a traditional architecture in [7], the detuning $\Delta_f = \omega_f - \omega_d$ affects the decay rather than $\Delta_r = \omega_r - \omega_d$, in this work, where ω_d is the drive frequency. Conceptually, in a readout circuit, the Purcell filter frequency, as the center frequency in a band-stop filter, should be selected close to the qubit frequency. This makes Δ_f to be an effective degree of freedom to manipulate κ_{eff} , as well as Δ_r which can be freely selected and therefore an effective quantity to strongly suppress the qubit decay.

The second term introduced in Eq. 3 is a determinative factor that has been missed out in the most of related studies including [3, 7]. This factor reveals that the average number of photons generated in the Purcell resonator affects the qubit's decay, generating an extra degree of freedom that this architecture presents. Another quantity is g which is the coupling strength rate between the qubit and Purcell filter, using which the decay rate can be manipulated. Addressing the mentioned equations, the new configuration offers several key advantages, which are critical in quantum circuit engineering. Firstly, the Purcell rate in this design depends primarily on the detuning of the readout resonator (Δ_r), a shift from traditional designs where the Purcell rate is mainly influenced by the filter resonator. This provides greater control over the system's performance, as the readout resonator's frequency can be more easily tuned for

optimal results. Secondly, unlike previous designs where the Purcell rate is influenced by the photon number in the main resonator, here, the number of photons in the filter resonator plays the primary role. So, by adjusting the photon number in the filter, we can further optimize the Purcell rate and enhance the system's stability. This capability is especially relevant for quantum systems requiring high precision, and high readout accuracy. This subtle yet crucial difference enhances the efficiency of the system, a point overlooked in many previous studies. Another interesting point is that there is no need to increase the readout resonator number of photons (n_r) to limit the Purcell decay in the system, since the critical photon number, n_{crit} , determines the level of non-classicality ($n_r \ll n_{crit}$) in the quantum system [7]. In the following, frequency difference as dispersive coupling ($2\chi = \omega_r^{|e\rangle} - \omega_r^{|g\rangle}$) generated by the coupling of the qubit-Purcell filter in the readout resonator is theoretically derived using the first- and the second-order perturbation theory. So, it is necessary to calculate $E^{|g\rangle} = E_0^{|g\rangle} + E_{int}^{(1)|g\rangle} + E_{int}^{(2)|g\rangle}$ and in the same way for $E^{|e\rangle}$. Thus, the readout resonator frequency when the qubit is in the ground state using the perturbation theory becomes:

$$\begin{cases} \omega_r^{|g\rangle} = E_{|g,n,m+1\rangle} - E_{|g,n,m\rangle} \longrightarrow \omega_r^{|g\rangle} = \Delta_r + \frac{|g_k|^2}{\Delta_r - \Delta_f} \\ \omega_r^{|e\rangle} = E_{|e,n,m+1\rangle} - E_{|e,n,m\rangle} \longrightarrow \omega_r^{|e\rangle} = \Delta_r + \frac{|g_k|^2}{\Delta_r - \Delta_f} - \frac{|g_k|^2}{\Delta_r + \Delta_f} \end{cases} \longrightarrow 2\chi = \omega_r^{|e\rangle} - \omega_r^{|g\rangle} = \frac{|g_k|^2}{\Delta_r + \Delta_f} \quad (4)$$

where $|g,n,m\rangle$ and $|e,n,m\rangle$ are various states of the system in which $|g\rangle$ and $|e\rangle$ are the ground and excited states of the qubit, respectively, $|n\rangle$ is a Fock state with n photons in the Purcell filter, and $|m\rangle$ is a Fock state with m photons in the readout resonator. The parameter 2χ derived theoretically for the new design differs significantly from traditional designs [7]. As discussed widely in the literature, 2χ (ac Stark factor) is a key parameter for distinguishing qubit states in the resonator's output, making it essential to design a system where 2χ can be manipulated efficiently. In this proposed design, 2χ is highly sensitive to g_{RF} , the coupling strength between the readout resonator and the filter, meaning that adjustments to g_{RF} directly impact the qubit state detection. A major advantage of this system is that tuning the resonator-filter coupling strength is relatively straightforward, offering flexibility in fine-tuning 2χ . Additionally, 2χ shows an inverse dependence on $(\Delta_r + \Delta_R)$, which contributes to the generation of a four-wave

mixing state. This mixing plays a critical role in frequency-selective measurements and ensures that non-ideal signal interactions are minimized, supporting clearer qubit state identification. Another significant improvement is the ability to achieve higher fidelity in the readout process. By modifying the coupling architecture, we found that the new design allows for a much more accurate transfer of quantum information, which is vital for high-performance quantum systems. This improvement in readout fidelity was confirmed through simulations. Indeed, QuTip in Python [23] is utilized to solve the Lindblad master equation, simulating the dynamics of the open quantum system interacting with its environment. The results were compared to those from traditional Purcell filter designs, and the new design consistently outperformed the earlier reports in terms of output fidelity.

3. Results and Discussions

This section initially focuses on studying the design dynamics in detail. However, a complete quantum circuit simulation conducted in CAD is provided in the Appendix A, where we demonstrate the performance of the new design. Fig. 2 illustrates the simulation results of a qubit-resonator system, with initial and final states analyzed in terms of coherent state representation and Fock state occupation probability. In Fig. 2(a), the initial state is shown as a coherent state centered around the origin in the complex plane, with a Gaussian distribution in both real $\text{Re}(\alpha)$ and imaginary $\text{Im}(\alpha)$ parts of the wave function. Fig. 2(b) provides the occupation probability in the Fock space, indicating that the system initially occupies the first Fock state predominantly. Fig. 2(c) and Fig. 2(d) show the final qubit states in two different designs (traditional design [7] and new design are labeled, respectively, Sys I and Sys II), suggesting minimal change from the initial coherent state, as the central distribution remains similar. These results indicate stable state evolution and preserved coherence across both configurations. Similarly, Fig. 2(e) and Fig. 2(f) illustrate the final resonator states for Sys I and Sys II, which also exhibit a Gaussian distribution with a high variation in Sys I. These results highlight that Sys II maintain coherence much better than the traditional architecture, likely preserving the initial state characteristics while potentially optimizing readout fidelity or suppressing decoherence mechanisms. Average fidelities of the

resonator for Sys I, Sys II and qubit are 0.8878, 0.9624, and 0.9981, respectively.

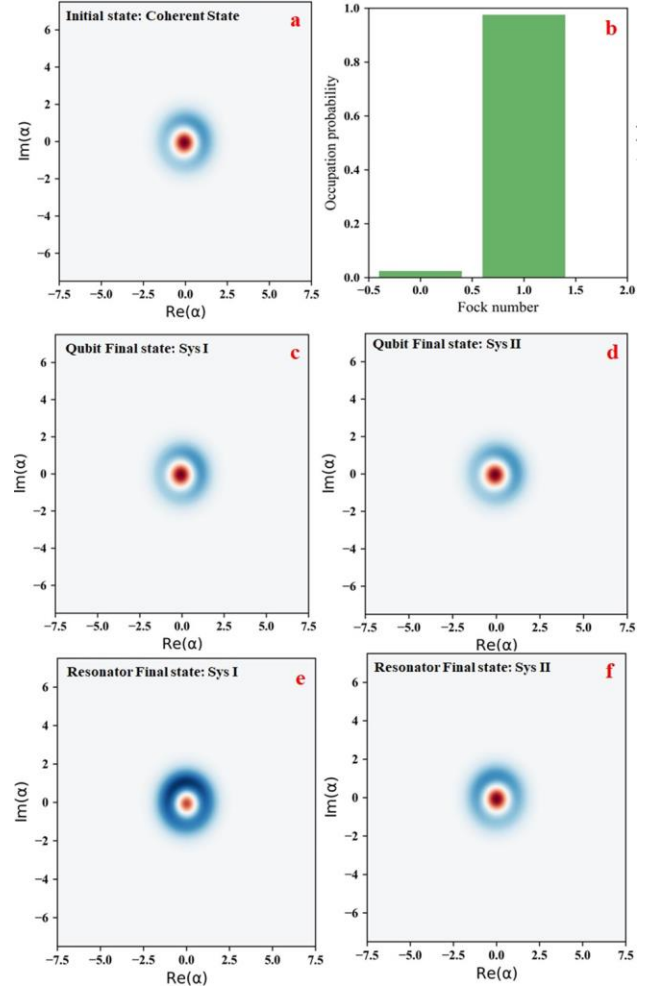


Fig 2. Simulation results showing the initial and final states of a qubit-resonator system. (a) The initial state depicted as a coherent state in phase space, with (b) its occupation probability in the Fock basis, (c) and (d) final qubit states for two different configurations, 'Sys I' and 'Sys II,' respectively, with minimal deviation from the initial state. (e) and (f) corresponding final resonator states for Sys I and Sys II. Data used: $\omega_r = 2\pi \times 6.6e9$, $\omega_f = 2\pi \times 6.328e9$, $\omega_q = 2\pi \times 6.313e9$, $\omega_d = 2\pi \times 6.310e9$, $g_k = 0.08 \times (\omega_r - \omega_f)$, $g = 0.01 \times (\omega_r - \omega_q)$, $\kappa_f = 0.002 \Delta_r$, $\alpha = 1+j$ and $N_H = 2$, where α and N_H represents the coherent state coefficient and number of Hilbert space, respectively.

Fig. 3 shows the fidelity of the resonator state (a) and qubit state (b) as a function of time and detuning frequencies, Δ_r and Δ_q respectively. Fidelity is a measure of how accurately the system maintains its initial state over time [24]. In both subfigures, the fidelity initially

remains high across a range of detunings but begins to show significant degradation, particularly strongly in the resonator around the detuning frequency $\Delta r \approx -0.3$ GHz and in the qubit in the range of $\Delta q \approx -0.2$ to 0.2 GHz. This descent is due to energy exchanges or coupling effects between the qubit and resonator. Detuning impacts the fidelity because it shifts the resonance alignment, impacting the coherence of the states. Optimal fidelity maintenance requires fine-tuning of the detuning frequency to minimize off-resonance interactions that lead to decoherence. However, we believe that the sharp variations in the fidelity (black-dashed rectangle on sub-figure 3a) is due to the decreasing the nonclassicality in the circuit. To clarify this point, the entanglement between the readout resonator and Purcell filter output is studied as follow.

Fig. 4 illustrates the entanglement criterion 2η [21] between the resonator and filter modes as a function of time and detuning frequency Δr . The parameter 2η serves as an indicator for the level of entanglement, with values $2\eta < 1$ as a certain threshold signifying non-classicality between modes. The plot shows that 2η varies notably with detuning frequency, reaching peak values around $\Delta r \approx -0.3$ GHz, where the resonator and filter modes appear maximally separable. In other words, a noticeable drop in fidelity, as observed in the previous figure may be linked to regions of high 2η , indicating a temporary loss of entanglement. Such dynamics suggest that the fidelity loss is related to the state entanglement, likely due to decoherence or phase shifts arising from detuning conditions.

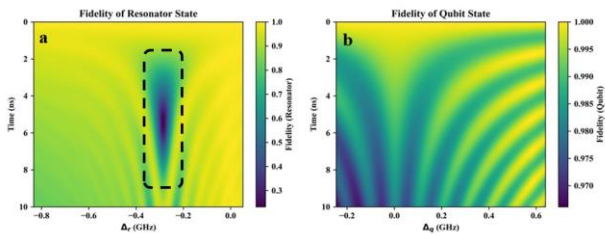


Fig 3. Time evolution of fidelity in the (a) resonator and (b) qubit states as a function of detuning frequencies (Δr and Δq). The figures highlight regions of high fidelity and a significant fidelity drop, indicating non-classicality disappearing.

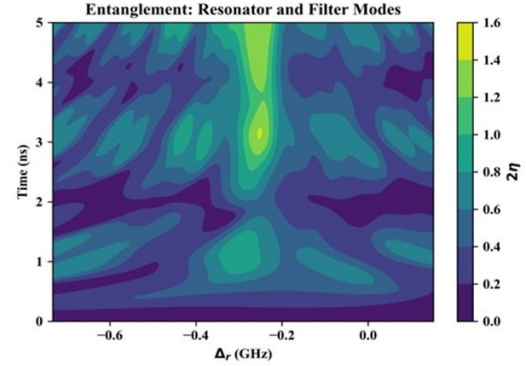


Fig 4. Evolution of the entanglement criterion 2η between resonator and filter modes as a function of detuning frequency Δr and time. High separability regions indicate strong dropping in fidelity near $\Delta r \approx -0.3$ GHz.

To deeply investigate the above-mentioned point, it is necessary to focus on Eq. 4 and study the effects of the critical parameters on the nonclassicality generated in the designed circuit. Through literature survey, it is found that there are a lot of versatile methods and approach to study the nonclassicality or quantum correlation in a quantum system; some bold utilized criteria are the Symplectic eigenvalue (2η) [21, 27], Peres-Horodesky-Simon (λ_s) [25-27], the entanglement metric (\mathcal{E}_e) and quantum discord [22, 28-30]; however, the reader may find other reported criteria as well. This work centers on methods or criteria that clarify the considered points of view; therefore, no judgement is made here about the validity or precision of those approaches.

It should be noticed that the main goal of this work is to find compromises existing between the 2χ increasing and the quantum correlation. In other words, we attempt to find out any connection between the quantities indicated. And answer to this question what happens on non-classicality as 2χ increases? Since it is found that 2χ is necessary in the readout circuit to get to know which states is which.

Here we choose the symplectic eigenvalue, entanglement metric, and quantum discord criteria to investigate the quantum entanglement. Symplectic eigenvalues and entanglement metric, in one hand, are mathematical constructs arising in the study of the phase-space structure of quantum states, particularly for Gaussian states in continuous-variable quantum systems [25-27]. They come from the symplectic diagonalization of the covariance matrix, which encodes information about the state's quadrature correlations. This criterion is used to calculate

properties such as entanglement entropy or logarithmic negativity, which are measures of entanglement—a specific type of quantum correlation [27]. In the other hand, quantum discord is a measure of quantum correlation that goes beyond entanglement. It quantifies the difference between two natural generalizations of classical mutual information in the quantum regime [29-30]. It arises from the fact that in a bipartite quantum system, the total correlations include both classical and quantum contributions, and quantum discord isolates those correlations that are inherently quantum but do not require entanglement. Quantum discord captures all quantum correlations, including those that are present even in separable (non-entangled) states. It thus provides a more general measure of quantum correlations than methods with measures purely based on entanglement. The dynamics of a quantum system consists of three coupled subsystems (Fig. 1): a qubit, a readout resonator, and a filter resonator. The system dynamics is modeled using the density matrix formalism, enabling the study of various quantum phenomena such as entanglement, quantum discord, and other indicators of nonclassicality. Each subsystem is described within a truncated Hilbert space of size N_{HN} . Key parameters include the frequencies of the subsystems, corresponding detunings, and coupling strengths. Coherent and thermal states are used to initialize the density matrix (ρ_0), which describe the mixed quantum state. The Hamiltonian of the system is constructed by summing the contributions of the individual subsystems (H_0), the interaction between subsystems ($H_{\text{int},s}$), the environment, and subsystem-environment interactions. Notably, detunings (Δ) and coupling strengths (g and g_k) determine the strength of interactions between components. Collapse operators are defined to incorporate dissipative effects, accounting for the interaction of the resonator, filter, and qubit with their respective environments. Using full Hamiltonian and collapse operators, the Lindblad master equation is employed using QuTip [23] to compute the time evolution of the system's density matrix, providing insights into the dynamics of quantum states. For analysis, various expectation values are extracted to analyze the quantum behavior of the system including the essential operators, annihilation and creation for the resonator (a_m, a_m^\dagger), filter (b_m, b_m^\dagger), and qubit (σ_m, σ_p). These operators are used to compute correlations, such as number operators (n) and cross-correlations between subsystems, which provide a foundation for assessing coherence, entanglement, and other nonclassical effects. Additionally, covariance

matrices are constructed from these expectation values to analyze joint quantum properties across subsystems. Covariance matrices are essential tools in quantum mechanics, particularly in the study of continuous variable (CV) systems [25-27], as they encapsulate information about the second-order moments of quantum operators. In this work, the covariance matrices are utilized to characterize the quantum states of subsystems, allowing the evaluation of nonclassical features such as entanglement, coherence, and quantum discord. For a Gaussian state, the covariance matrix provides a complete description of the quantum system. This completeness arises because the state is fully specified by its first and second moments. While the first moments (e.g., $\langle X \rangle, \langle P \rangle$) describe the mean displacement, the covariance matrix encapsulates all information about the quantum fluctuations and correlations. In the case of non-Gaussian states, additional higher-order moments are required for a complete description [26-28]. However, the covariance matrix still serves as a critical foundation for approximations and partial characterizations. Finally, we calculate the consequent metrics to quantify nonclassicality, including quantum discord, entanglement metric, entanglement metric (\mathcal{E}_e), and symplectic eigenvalue (2η). The covariance matrices for the resonator, filter, and their cross-correlations are pivotal in assessing these properties. These metrics are evaluated at each time step, capturing the dynamic evolution of nonclassical features in the system.

Analyzing Eq. 3 and Eq. 4 suggests that a few critical parameters such as g_k , κ_f , Δ_r , and Δ_f influence the qubit decay and more importantly affect 2χ . Therefore, in the following we attempt to investigate their effects on the nonclassicality generated by the circuit.

In Fig. 5, the entanglement is characterized by the entanglement metric ($\mathcal{E}_e = N_{\text{RF}}/\sqrt{(N_{\text{R}} \times N_{\text{F}})}$, where N_{R} , N_{F} , and N_{RF} are the readout resonator average photon number, Purcell filter average photon number, and the cross-correlation between the readout resonator and Purcell filter, respectively.) representing the interaction between the resonator and filter modes. The periodic variation in \mathcal{E}_e reflects the recurring entanglement between the resonator and filter modes over time. The decay of the oscillations indicates energy dissipation into the environment, possibly due to photon leakage or qubit dephasing. This interplay between coherent quantum dynamics and dissipation is typical in open quantum systems. It is interesting to notice that the quantum system depicted in Fig. 1 demonstrates some interaction among subsystems,

causing the states to become mixed. Consequently, quantum discord was adopted as the criterion for assessing quantum correlations instead of entanglement.

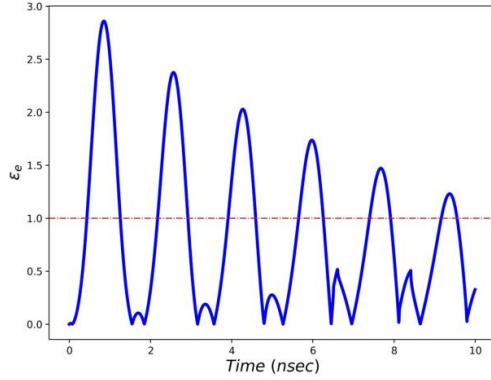


Fig. 5 Time Evolution of the entanglement (symplectic eigenvalue) between resonator and filter modes; $\kappa_r = 0.001\omega_r$, $g = 0.01 \times (\omega_r - \omega_q)$, $g_k = 0.01 \times (\omega_r - \omega_f)$, $\kappa_f = 0.002\Delta_r$, the initial state is the coherent state with $\alpha = 0.5 + 0.07j$ and $N_H = 2$; the horizontal line indicates the entanglement metric limit, where $\mathcal{E}_e > 1$ means entangled modes.

In Fig. 6a, the quantum discord is plotted as a function of g (the coupling strength between the qubit and filter) and g_k (the coupling strength between the resonator and filter). The bands of higher quantum discord (depicted in yellow) indicate parameter regions where the system exhibits stronger quantum correlations between the resonator and filter modes. These regions suggest optimal coupling strengths where the interplay between the components enhances entanglement-like behavior, demonstrating how precise tuning of g and g_k can maximize quantum information sharing in the system. In addition, the sinusoidal shadow on Fig. 6a may arise from periodic constructive and destructive interference between the coupling strengths g and g_k . Such interference is a hallmark of resonant systems where the frequencies of coupled components are tuned to specific ratios, leading to oscillatory behaviors in quantum correlations like quantum discord. This shadow emphasizes the delicate interplay between coupling parameters and system dynamics, highlighting regions where quantum coherence and correlations are suppressed.

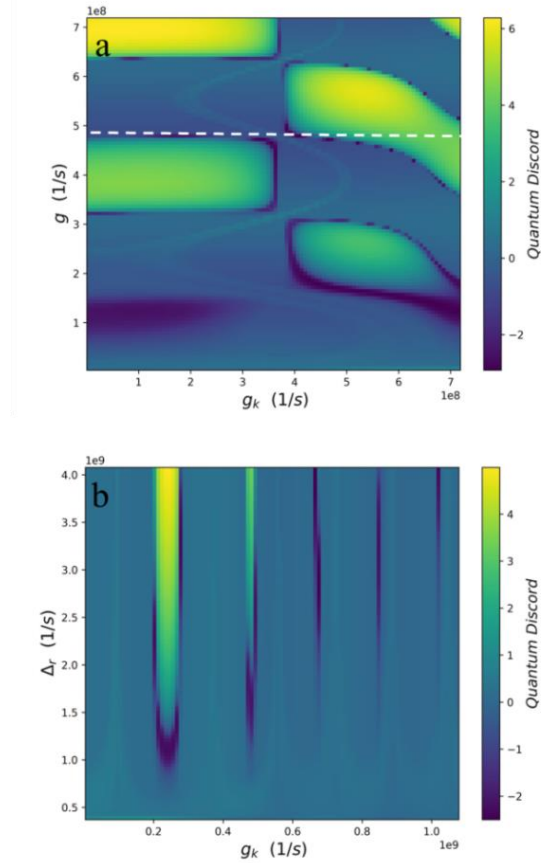


Fig. 6 2D illustration of quantum discord for resonator and filter modes; $\kappa_r = 0.001\omega_r$, $\kappa_f = 0.002\Delta_r$, the initial state is the coherent state with $\alpha = 0.5 + 0.07j$ and $N_H = 2$.

Along with, Fig. 6b explores quantum discord as a function of g_k and Δ_r (the detuning between the resonator and drive) for $g = 0.01 \times (\omega_r - \omega_q)$. The vertical bands of high quantum discord reflect resonances where specific values of g_k and Δ_r align to strengthen quantum correlations. The periodicity in these bands implies that the system's quantum behavior is sensitive to detuning. In other words, one can create constructive interference that boosts discord with certain detuning values. Together, these plots emphasize the critical role of system parameters, including coupling strengths and detunings, in controlling quantum correlations, making them valuable degrees of freedom as design considerations in circuit QED experiments for quantum information processing.

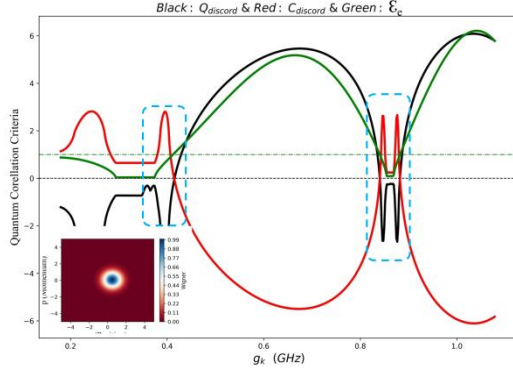


Fig. 7 Comparison among quantum discord, classical discord, and \mathcal{E}_e vs g_k ; the initial state is the coherent state with $\alpha = 0.5 + 0.07j$ and $g = 4 \times 10^8 \text{ s}^{-1}$.

Fig. 7 illustrates the comparison between the quantum discord (Q_{discord} , black curve), classical discord (C_{discord} , red curve), and the symplectic eigenvalue (\mathcal{E}_e , green curve) as functions of g_k for a fixed $g = 4 \times 10^8 \text{ s}^{-1}$, which is corresponding to the vertical white dashed line in Fig. 6a. The green dashed line indicates the entanglement metric limit for nonclassicality ($\mathcal{E}_e < 1$ means modes separability), while the black line reveals the threshold for quantum discord ($Q_{\text{discord}} > 0$ means nonclassicality between modes). The behavior of these quantities reveals intricate dynamics in the system. The green curve (\mathcal{E}_e) showcases oscillatory behavior, reflecting the resonator-filter entanglement dynamics. Meanwhile, the quantum discord and classical discord exhibit distinctive peaks and dips, indicating regions where quantum and classical correlations dominate, respectively. Interestingly, the classical discord's peaks occur at points of significant change in quantum discord, emphasizing the complementary nature of these measures. The sky-blue rectangles on the graph show locations where the sinusoidal shadow on Fig. 6a pass through it. Along side, the inset Wigner function illustrates the phase-space representation of the initial state, suggesting coherence and non-classicality as contributing factors to the observed correlations. This comparison underscores the nuanced interplay between quantum and classical correlations in this coupled quantum system.

In Fig. 8, the effect of the initial state is studied; investigating how much the quantum correlation will get affected if the initial state of the subsystems is varied from the coherent state into thermal state. In contrast to the latter results depicted in Fig. 7, which shows the separability between modes for the most g_k . Apparent

from the figure, in the case of just strong coupling between modes, the entanglement can be happened. This result is certified by the quantum discord results (black curve). It shows that for $g_k < 0.96 \times 10^8 \text{ s}^{-1}$ the behavior of modes is classic completely.

Finally, the challenging question persists: to what extent is the nonclassicality affected after passing through the Josephson Parametric Amplifier (JPA)? [31-33]. It is because JPA is an indispensable component in a quantum circuit. This is the novel subject that any quantum circuit engineers need to know about.

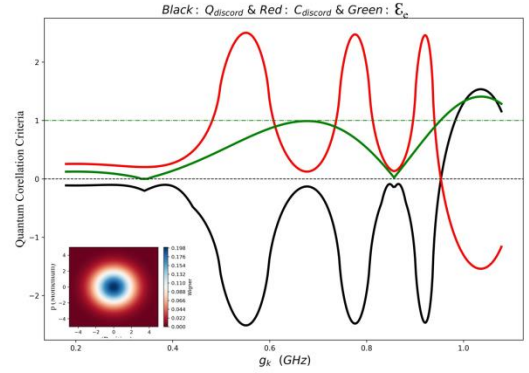


Fig. 8 Comparison among quantum discord, classical discord, and \mathcal{E}_e vs g_k ; the initial state is the thermal state with $n_{\text{th}} = 2$ and $g = 4 \times 10^8 \text{ s}^{-1}$.

4. Conclusions

In this work, we introduced a novel qubit readout circuit design to effectively suppress the Purcell effect, which is a major challenge in maintaining high fidelity in qubit-resonator systems. This design enables precise control over the Purcell decay rate, allowing for improved qubit state measurements without compromising entanglement or increasing measurement time. Unlike traditional circuits, this configuration offers a new degrees of freedom by enabling flexible tuning of the coupling strength and photon number in the filter resonator, enhancing readout fidelity and stability. Simulation results demonstrate improved coherence and stability in qubit states, with optimized fidelity under specific detuning conditions. This ability to maintain high fidelity and entanglement in quantum systems is crucial for advancing scalable, reliable quantum computing architectures where minimizing energy leakage is essential. In addition, the results indicate that optimizing the coupling strengths and system parameters

significantly improves quantum correlation and nonclassicality of the output signals, as evidenced by the behavior of quantum discord, classical discord, and the symplectic eigenvalue. Specifically, the analysis reveals that the quantum discord surpasses classical discord across various coupling strengths, underscoring the preservation of quantum correlations in the proposed system. Furthermore, the system achieves robust nonclassicality, as shown by the dynamics of the symplectic eigenvalue, which remains consistent with expected quantum behaviors. These results highlight the ability of the proposed design to balance efficient state readout and nonclassicality preservation, making it a promising solution for scalable quantum architectures.

References

- [1] Blais A, Huang R S, Wallraff A, Girvin S M and Schoelkopf R J 2004 *Phys. Rev. A* **69** 062320.
- [2] Purcell E M, Torrey H C and Pound R V 1946 *Phys. Rev.* **69** 37.
- [3] Sete E A, Gambetta J M and Korotkov A N 2014 *Phys. Rev. B* **89** 104516.
- [4] Houck A A et al 2008 *Phys. Rev. Lett.* **101** 080502.
- [5] Gambetta J, Braff W A, Wallraff A, Girvin S M and Schoelkopf R J 2007 *Phys. Rev. A* **76** 012325.
- [6] Koch J et al 2007 *Phys. Rev. A* **76** 042319.
- [7] Sete E A, Martinis J M and Korotkov A N 2015 *Phys. Rev. A* **92** 012325.
- [8] Schuster D I et al 2007 *Nature* **445** 515.
- [9] DiCarlo L et al 2009 *Nature* **460** 240.
- [10] Chow J M et al 2010 *Phys. Rev. A* **81** 062325
- [11] Salmanoglu A 2023 *Phys. Lett. A* **479** 128925
- [12] Dou F Q and Yang F M 2023 *Phys. Rev. A* **107** 023725.
- [13] Wei K X, Lauer I, Pritchett E, Shanks W, McKay D C and Javadi-Abhari A 2024 *PRX Quantum* **5** 020338.
- [14] Reed M D et al 2010 *Appl. Phys. Lett.* **96** 203110.
- [15] Jeffrey E et al 2014 *Phys. Rev. Lett.* **112** 190504.
- [16] Gambetta J M, Houck A A and Blais A 2011 *Phys. Rev. Lett.* **106** 030502.
- [17] Bronn N T, Magesan E, Masluk N A, Chow J M, Gambetta J M and Steffen M 2015 *IEEE Trans. Appl. Supercond.* **25** 1.
- [18] Sah A, Kundu S, Suominen H, Chen Q and Möttönen M 2024 *Commun. Phys.* **7** 1.
- [19] Scully M O and Zubairy M S 1997 *Quantum Optics* (Cambridge: Cambridge University Press).
- [20] Salmanoglu A and Geçim H S 2020 *IEEE J. Sel. Top. Quantum Electron.* **26** 4600110.
- [21] Salmanoglu A, Gokcen D and Geçim H S 2019 *Phys. Rev. Appl.* **11** 024075.
- [22] Salmanoglu A 2022 *Quantum Sci. Technol.* **7** 045026.
- [23] Johansson J R, Nation P D and Nori F 2013 *Comput. Phys. Commun.* **184** 1234.
- [24] Jozsa R 1994 *J. Mod. Opt.* **41** 2315.
- [25] Ge W, Tasgin M E and Zubairy M S 2015 *Phys. Rev. A* **92** 052328.
- [26] Simon R 2000 *Phys. Rev. Lett.* **84** 2726.
- [27] Tasgin M E 2015 arXiv:1502.00992 [quant-ph].
- [28] Salmanoglu A 2023 *Opt. Quantum Electron.* **55** 745.
- [29] Barzanjeh S, Guha S, Weedbrook C, Vitali D, Shapiro J H and Pirandola S 2015 *Phys. Rev. Lett.* **114** 080503.
- [30] Barzanjeh S, Pirandola S, Vitali D and Fink J M 2020 *Sci. Adv.* **6** eabb0451.
- [31] Salmanoglu A, Zandi H and Akbari M 2024 *IEEE J. Sel. Top. Quantum Electron.* in press <https://doi.org/10.1109/JSTQE.2024.3522509>
- [32] Planat L 2020 *Resonant and Traveling-Wave Parametric Amplification Near the Quantum Limit* PhD dissertation, Univ. Grenoble Alpes.
- [33] Eichler C and Wallraff A 2014 *EPJ Quantum Technol.* **1** 2.

DATA AVAILABILITY

The data that supports the finding of this study are available from the corresponding author upon reasonable request.

CONFLICT OF INTERESTS

There is no any conflict of interests.

Appendix A:

The quantum circuit shown in Fig A1, represents a schematic of the proposed transmon qubit readout system designed for quantum computing applications. The main components in this circuit include the transmon qubit, Purcell filter resonators, readout resonators, and coupling capacitors. Each component is intricately designed and tuned to specific frequencies to ensure optimal interaction and performance. The inset table provides simulation results obtained by CAD software, highlighting the resonance frequencies, anharmonicities, and cross-Kerr effects among these components. The transmon qubit is positioned in center and coupled to surrounding elements through strategically placed coupling capacitors. The Purcell filter resonators are included to mitigate the Purcell decay effect, which can adversely affect the qubit's coherence by increasing its decay rate into the readout circuit. The readout resonator is responsible for detecting the state of the qubit and connected through coupling components for controlled interaction. Each resonator adjacent to the qubit is designed as a high-quality microwave circuit with distinct resonance frequencies to prevent undesired interactions and overlaps in their operating spectra.

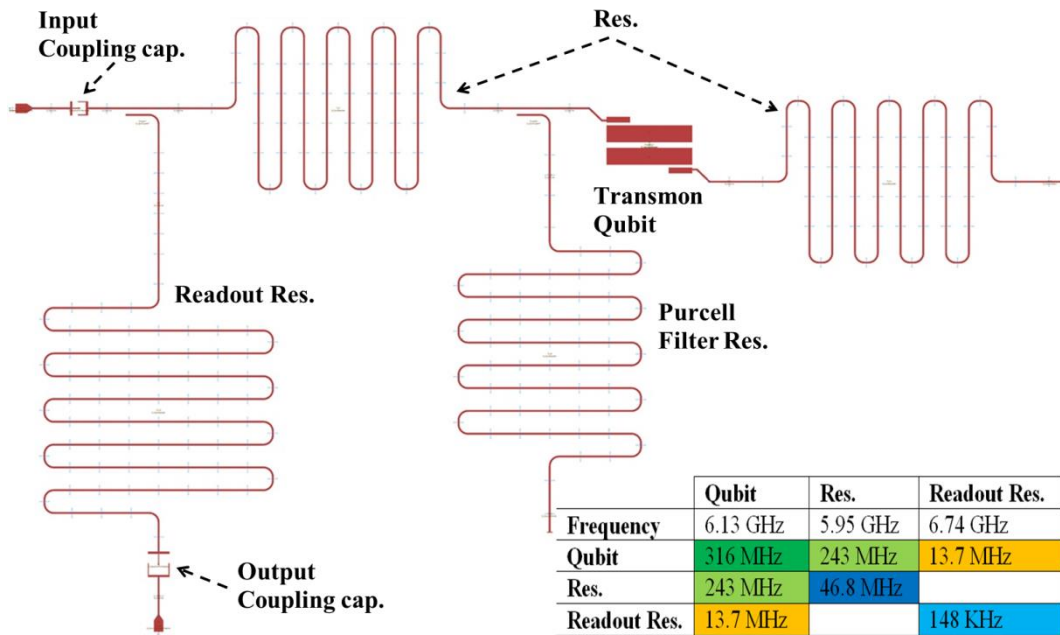


Fig A1. Quantum circuit schematic (called Sys II in the main article) with transmon qubit, Purcell filter resonators, and readout resonators. The inset table presents resonance frequencies, anharmonicities (qubit: dark-green, Res: dark-blue, readout Res: light-blue), and cross-Kerr interactions (qubit-Res: light-green, qubit-readout Res: orange), illustrating the circuit's optimized design for elevated coherence and also precise state measurement.

The transmon qubit operates at a resonance frequency of 6.13 GHz with an anharmonicity of 316 MHz. This level of anharmonicity is crucial to distinguish the qubit states ($|0\rangle$ and $|1\rangle$) from higher energy states and reducing gate errors during quantum operations. The Purcell filter resonators work around 6.13 GHz, slightly differ (higher or lower) from the qubit's resonance frequency with a suitable bandwidth, to suppress qubit energy decay into the environment effectively. The readout resonator, with a central frequency of 6.74 GHz, is well-separated from both the qubit and Purcell filter resonances. This separation, combined with its anharmonicity of 0.148 MHz, minimizes cross-talk and facilitates a much more precise qubit state measurement. The cross-Kerr effect between the various components indicates that the interaction strength and coupling-induced frequency shifts, while the cross-Kerr coupling between the qubit and the Purcell resonators are very strong. The readout resonator and qubit cross-Kerr coupling is set as 13.7 MHz, demonstrating weak coupling, ensuring that the readout process does not significantly disturb the qubit's state. The qubit-Purcell filter interaction shows sufficient coupling to strongly suppress the Purcell decay rate. Consequently, the carefully designed resonance frequencies and anharmonicities indicate precise engineering to meet the demands of quantum computation. The Purcell filters play a critical

role in protecting qubit coherence, while the weak cross-Kerr coupling to the readout resonator ensures accurate state measurement without back-action on the qubit. Additionally, the design showcases the careful balancing of coupling strengths through the coupling capacitors, which directly influence the circuit's performance.

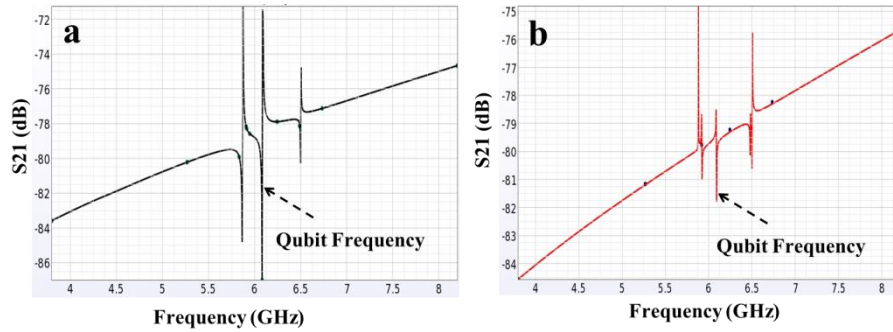


Fig A2. (a) Transmission spectrum (S_{21}) without a Purcell filter, showing a clear qubit resonance frequency around 6.13 GHz. (b) Transmission spectrum (S_{21}) with a Purcell filter, demonstrating suppression of the qubit resonance frequency.

The Purcell filter plays a critical role in protecting the coherence and stability of qubits in quantum circuits by mitigating the Purcell effect, a phenomenon which explains the qubit state's energy decay into the readout or coupling resonator. Illustrated in Fig A2a, the qubit resonance frequency in the absence of a Purcell filter is prominently visible in the transmission spectrum (S_{21}). This is characterized by a sharp dip in the spectrum at the qubit's resonance frequency (approximately 6.13 GHz). When the Purcell filter is integrated into the quantum circuit (Fig. A2b), the qubit resonance frequency is suppressed, as shown in the plot, while the readout resonator frequency is not affected. The Purcell filter effectively blocks the undesired energy leakage by introducing a frequency-selective element that attenuates the qubit's resonance. This suppression ensures better isolation of the qubit, enhancing its coherence time without sacrificing the overall system performance. The suppression of the qubit resonance frequency in the presence of the Purcell filter demonstrates its efficacy in minimizing qubit decay while maintaining high readout fidelity. The study highlights the importance of precise filter design, particularly in tuning the resonant properties of the filter to match the operational requirements of the quantum system. This work underscores the utility of Purcell filters in scalable quantum systems requiring long coherence times and efficient readout mechanisms.